TWENTE UNIVERSITY

MASTER THESIS

Robotic assisted open cranial vault reconstruction for craniosynostosis

Author:
BSc Jelle Man

Examination committee:
Dr. Marloes Nienhuijs,
Dr. Ir. Luc Verhamme,
Dr. Françoise Siepel,
Dr. Ferdi van der Heijden

3D lab Oral and maxillofacial surgery
RadboudUMC
Technical Medicine

May 4, 2021

TWENTE UNIVERSITY

Abstract

Technical Medicine

Robotic assisted open cranial vault reconstruction for craniosynostosis

by BSc Jelle Man

In some institutions open cranial vault reconstruction involves a virtual planning stage in which a computed tomography scan of the cranium of a patient is used to determine appropriate sawing lines to achieve a symmetric result, with fluent boundaries between the rearranged bone pieces, and with an intracranial volume created which is representative of kids their age. This virtual planning can be transferred to the skull by means of 3D printed patient specific molds or by identifying the planned sawing lines with the help of landmarks on the skull. As a method to transfer this planning in a more time efficient manner a robotic workflow is developed in this thesis. This is strived for because operating time is associated with the amount of blood lost during the procedure. Achieving a low amount of blood loss is of critical importance because of the typically high amount of blood loss during this surgical operation and the low circulating blood volume of these infants.

The requirements of a robotic workflow are first determined with the help of discussions with clinicians, obtained experience while participating in the current workflow, and a literature search. The developed robotic workflow is implemented within a simulated and simplified version of this operation. And an experiment is set up to validate the implemented workflow. An additional experiment is carried out to determine the relative contribution of each step in the workflow to the total error. The developed workflow consists of two programs, one which can be performed in the preparation stage of the surgical operation and one to perform the actual movements with respect to the skull. The mean Euclidean error of this implemented workflow is reported to be 3.9 mm ($\pm$ 0.79 SD), 4.0 mm ($\pm$ 1.1 SD) and 3.9 ($\pm$ 0.78 SD) for 3 distinct registration trajectories.

This error makes the robotic workflow in its current implementation and with the currently used materials not accurate enough for a clinical implementation. The relatively large inaccuracy of the Viper 850 robotic in determining its end effector pose is the cause of a large part of this error. It is recommended to replace the used industrial robot with a robot from which its internal parameters are determined with a higher precision and to use a stereo camera setup with higher lens magnification and a more narrow FOV so that the tracking system fits better for the surgical procedure.

Acknowledgements

Ik wil Marloes bedanken voor de nuttige feedback gedurende mijn klinische werk. Hier heb ik veel van geleerd over hoe ik mij opstel in de kliniek en wat ik hieraan wil verbeteren. Ook wil ik haar bedanken voor de prettige samenwerking tijdens het plannen en het helpen bij het uitvoeren van de craniosynostose operaties. Daarnaast wil ik Marloes en Jene allebei bedanken voor het betrekken van mij in het interessante klinische proces van het plannen van craniosynostose operaties en het geven van uitleg aan de ouders over de progressie van het herstel van de operaties aan de hand van 3D foto's. Ook wil ik Jene bedanken voor de uitnodiging om mijn afstudeerstage te doen binnen het 3D lab en voor de goede begeleiding en het uitgebreide overleg dat ik met hem kon voeren tijdens het eerste gedeelte van mijn stage.

Daarnaast wil ik Luc bedanken voor het overnemen van mijn technische begeleiding en omdat hij zich altijd beschikbaar stelde voor overleg over de opdracht of het nakijken van een gedeelte van mijn thesis en voor de vriendelijkheid die hij gedurende de stage aan mij getoond heeft. Ook wil ik hem bedanken voor de waardevolle input die hij gedurende het jaar geleverd heeft in de vorm van feedback aan mij of technische input voor mijn onderzoek. Ook wil ik Françoise bedanken voor het goede overleg wat we hebben gevoerd gedurende dit jaar. Voor de nuttige feedback op wat ik gedurende dit jaar van haar heb ontvangen. In het bijzonder voor de nuttige tips en feedback bij het schrijven van mijn thesis. Daarnaast wil ik haar bedanken voor het koppelen van mij aan personen in haar afdeling die mij op een uitgebreide manier konden helpen bij het oplossen van een technisch probleem. En voor de positiviteit en enthousiasme waarmee ze mij begeleid heeft.

Daarnaast wil ik Elyse bedanken voor de begeleiding die ze heeft gegeven gedurende mijn stages en het begin van deze stage. Ook wil ik haar bedanken voor dat ze mij geleerd heeft om op een wat neutralere, kritische, maar minder veroordelende manier naar mezelf te kijken. Daarnaast wil ik Paul bedanken voor de begeleiding van een groot gedeelte van deze afstudeerstage. De nuttige inbreng die hij gaf op zaken waar ik tegenaan liep tijdens mijn stage en doelstellingen die ik tijdens intervisiemomenten inbracht heeft me geholpen om naar mijn idee belangrijke progressie te maken op persoonlijk gebied en als technisch geneeskundige.

Ook wil ik Arico en Frank bedanken voor de ruimte die ze mij gaven om de technisch geneeskundige taken gerelateerd aan craniosynostose uit te voeren. En de nuttige feedback die ze daarbij aan mij gaven. Ook wil ik Thomas bedanken voor de betrokkenheid en intresse die hij getoont heeft in mijn stage. Daarnaast wil ik de medewerkers en de stagairs van het 3D lab bedanken voor de feedback die velen van jullie aan mij hebben gegeven tijdens de tussentijdse presentaties en daarbuiten en voor de gezellige momenten.

Contents

List of abbreviations mathematical symbols

3D	3 dimensional
DOF	Degrees of freedom
MRI	Magnetic resonance imaging
SD	Standard deviation
CT	Computed tomography
CBCT	Cone beam computed tomography
mm	milimeter
SDK	Software development toolkit
TCP/IP	Transmission control protocol / internet protocol
FRE	Fiducial Registration Error
FOV	Field of view

F_c	Frame of the stereo camera
F_0	Base frame of the robot
$\mathbf{H}_0^{PT}$	Transformation matrix to describe a pointer pose with respect to the robotic base frame
$\mathbf{H}_{PT}^{F}$	Transformation matrix to describe the flange pose with respect to the pointer pose
$\mathbf{H}_0^{F}$	Transformation matrix to describe the flange pose with respect to the robotic base frame
$\mathbf{H}_0^{C}$	Transformation matrix to convert poses expressed in camera frame to poses expressed in the robotic base frame
$\mathbf{H}_0^{D}$	Transformation matrix to convert a desired pose of the robot to the desired pose in base frame coordinates
$\mathbf{H}_C^{P}$	Transformation matrix to convert poses expressed in the frame of the planning to poses expressed in the frame of the tracking system
$\mathbf{H}_P^{D}$	Transformation matrix to convert a desired pose of the robot to to the coordinate frame in the operation planning software
$\mathbf{H}_D^{DF}$	Transformation matrix to describe the desired pose of the flange of the robot in the frame of the desired pose of the pointer
$\mathbf{H}_0^{\text{Home}}$	Transformation matrix to describe the Home pose with respect to the base frame of the robot
${}^{c}\mathbf{p}_{\text{origin}}$	The pose of the origin of the pointer expressed in the camera frame
k	The step integer in the for loop ranging from 1 to 5
xb	Vector of iterations at which the robot arrives at a target point
xb	Vector of iterations at which the robot leaves a target point

Chapter 1

Introduction

1.1 Clinical relevance

During infancy the bones of the cranial vault are separated by soft fibrous tissue called sutures. These sutures allow the bones of the cranial vault to keep growing throughout infancy and childhood. [1] Premature closure of these cranial sutures, called craniosynostosis, is affecting approximately 7.2 per 10.000 live born children in the Netherlands. [2] Left untreated the premature closure of sutures is associated with a distorted head shape and a higher risk of developing a variety of neurological, sensory, and respiratory symptoms. [3] The three most common types of craniosynostosis are scapocephaly, which is the premature closure of the saggital suture and is affecting an estemated 44% of all cases. Trigonocephaly, which is the premature closure of the metopic suture affecting an estimated 32% of all craniosynostosis cases. And plagiocephaly, which is the premature closure of the lambiod suture or one of the 2 coronal sutures affecting 11% of all cases. Premature closure of more than one suture occurs in an estimated 5% of all cases. [2] The types of craniosynostosis are depicted in figure 1.1

Because of the risks associated with the premature closure of the sutures it is generally recommended that the patients are treated surgically. [3] Endoscopic treatment is recommended for patients younger than 6 months. The diagnosis of craniosynostosis is however not always made before 6 months of age, due to that the parents and the other people in the environment of the infant do not recognize the abnormal skull shape in time. For children older than 6 months an open cranial vault remodeling is recommended. [5] In this surgical operation a large part of the cranium is reconstructed by removing large pieces of the skull, sawing these bone pieces into smaller ones and rearranging the bones to form the reconstructed skull.

In some institutions including RadboudUMC Nijmegen, this surgery involves a virtual planning stage in which a computed tomography scan of the cranium of a patient is used to determine appropriate sawing lines to achieve a symmetric result, with fluent boundaries between the rearranged bone pieces, and with an intracranial volume created which is representative of kids their age. [6] One of the advantages of making a preoperative virtual planning is that the result of multiple rearrangement can be examined before actually sawing into the bone. The sawing lines can thus be optimized prior to the operation by trying multiple sawing lines along the virtual cranium, rearranging the bone and analysing the result. Performing the surgery according to a virtual surgical planning is reported to reduce the total operating time and with that the intraoperative blood loss and anesthetic usages. [7] A reduction in blood loss is especially important in these small infants undergoing open skull reconstruction as a volume of blood loss which is considered moderate in adults can potentially lead to a critical hypotension in these infants requiring blood transfusions with their associated risks. [8, 9] Blood loss is in this

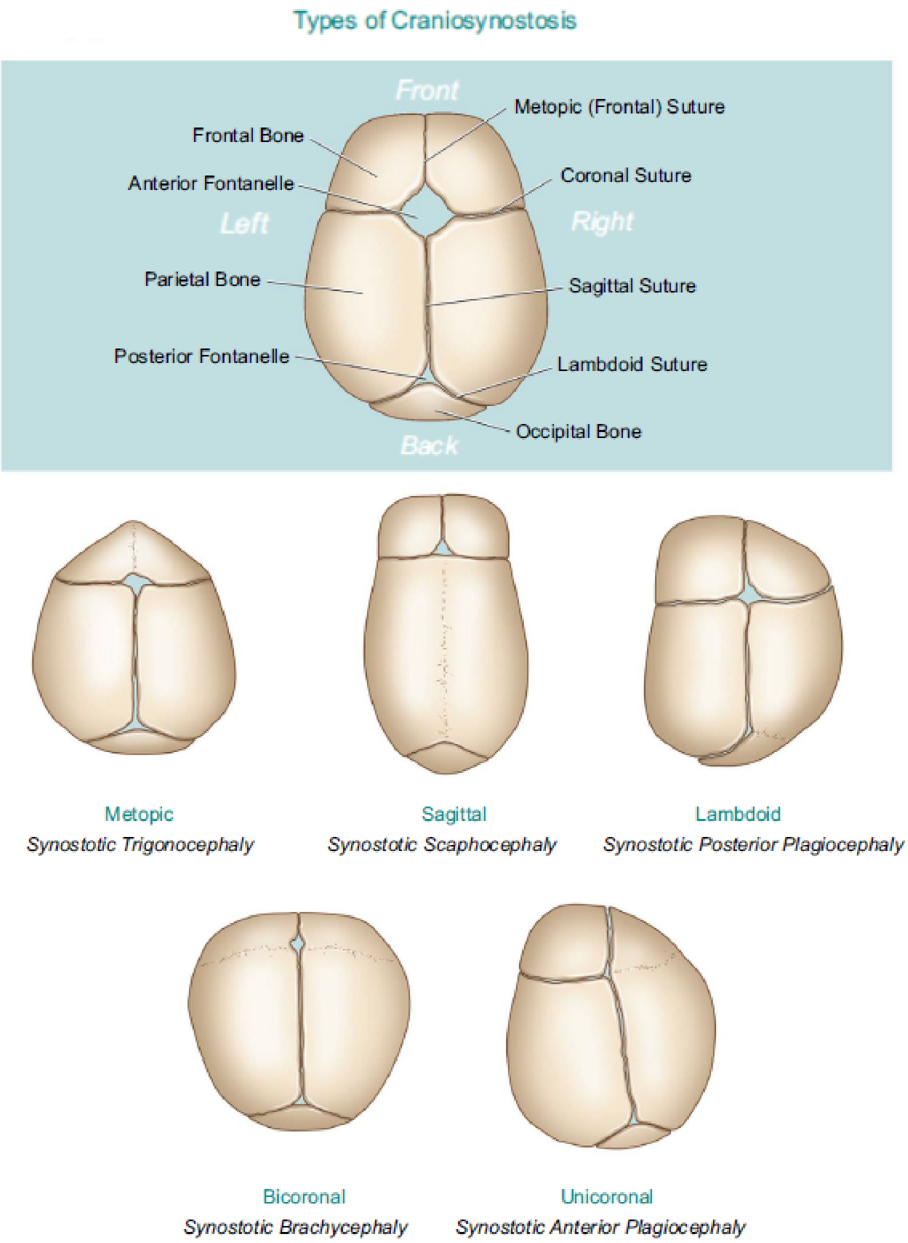

FIGURE 1.1: The anatomy of an infant's skull along with several types of craniosynostosis. [4]

operation is associated with an increase in morbidity and length of stay in the hospital. [8–10]

There are several ways to transfer the virtual planning to the skull of the patient including the conventional method to transfer the planning based on anatomical landmarks, transferring the planning onto the skull using augmented reality and using three dimensional (3D) printed patient specific templates. [6, 11] Using 3D printed patient specific templates is currently the golden standard due to its high precision in transferring the virtual planning and a reduction in the total operating time and intraoperative blood loss compared to the conventional method. [7, 11, 12] Using a template is however time intensive to develop and manufacture and costly, since every template needs to be developed, 3D printed and sterilized prior to every operation. The manufacturing and sterilization costs are between 2000-6000 euros and the development time is approximately 1-2 day. [13, 14]

This thesis is part of a larger project in which it is investigated if a robotic arm could be used to effectively transfer the virtual planning on a skull. This is investigated with the following goals. Reducing operating time, reducing the costs and development time per operation by eliminating the need for producing patient specific molds, and creating smoother sawing lines. A reduced surgical operating time with a robot is an obtainable goal since it would not be necessary to first fit a guide, then draw the patterns on the skull and then saw while closely following the drawn patterns. The robot would be able to saw these patterns directly without the need of marking the desired patterns first. A faster operating time would lead to less intraoperative blood loss and anesthetic usages. [9] Smoother sawing lines are expected to make the surgical result more closely resemble the 3D planning and improve the aesthetic outcome as uneven bone pieces generally fit together less well than bone pieces created from smooth and even sawing lines.

1.2 Research aim

In this thesis a workflow is designed for implementing a robotic arm with 6 degrees of freedom (DOF) within an open cranial vault reconstruction. The workflow is implemented and the error of in the workflow is tested with the PST base HD (PS-tech, Amsterdam, The Netherlands) and a Viper 850 robot (Omron, Kyoto, Japan). These components are integrated in a way in which it is possible to send poses of objects detected by the tracking system to the robot in the robotic base frame, so that the robot can move to detected targets and adapt its movements based on movements of the patient. In order to make this possible the coordinate system of the robot, the tracking system and the virtual planning need to be aligned with one another. This needs to be done in a way in which this alignment procedure would be suitable for usage during a surgical operation in terms of the time required to perform the alignment procedure and the stage of the operation in which it can be performed. It is investigated if the proposed workflow can be used to accurately transfer virtual cutting patterns on a 3D printed skull detected by the PST base HD tracking system and in what way the current setup needs to be improved to bring this workflow into practice.

1.3 Outline

The relevance of the project and the research aims of the thesis are explained in the introduction. Chapter 2 gives more information about the current surgical workflow of craniosynostosis surgery. Chapter 3 provides an explanation of the working principles of surgical robots in a operating theater, and gives an overview of the levels of autonomy of surgical robots. Chapter 4 is the method section in which it is described how the workflow is developed. The setup of the experiments done to validate the workflow in this current implementation is also described. The developed workflow and the results of the validation experiments are described in chapter 5. Chapter 6 is the discussion section of this thesis, and in chapter 7 the conclusion is given.

Chapter 2

Current surgical workflow

The current interaoperative process can be divided into 7 steps as illustrated in figure 2.1 and listed in more detail below.

1. The operation begins with the surgeons moving the tissue layers aside to expose the portion of the cranium necessary for the bone reconstruction.
2. Then the preoperatively determined sawing lines are drawn on the bone using a patient specific 3D printed template.
3. Large bone pieces are removed by first using a surgical drill at a selected place to make a small hole. The bone is subsequently removed by sawing from the small hole outwards while following the pattern drawn on the skull.
4. The bone pieces are then sawed in smaller pieces as indicated by the drawn sawing lines.
5. These smaller bone pieces are fitted into the correct shape as determined by the preoperative planning and with the help of a patient specific fitting guide. The pieces are attached to one another using biodegradable material.
6. This step involves placing the reconstructed skull pieces back on to the patient and attaching the reconstructed pieces to the rest of the skull.
7. Lastly the reconstructed calvarium is covered with its original tissue layers.

A robot can be used to draw sawing patterns (step 2) and in a later stage saw the larger bone pieces out of the skull (step 3). It can also be used to saw the larger bone pieces into smaller pieces (step 4) and for attaching the smaller bone pieces to one another in the correct arrangement (step 5).

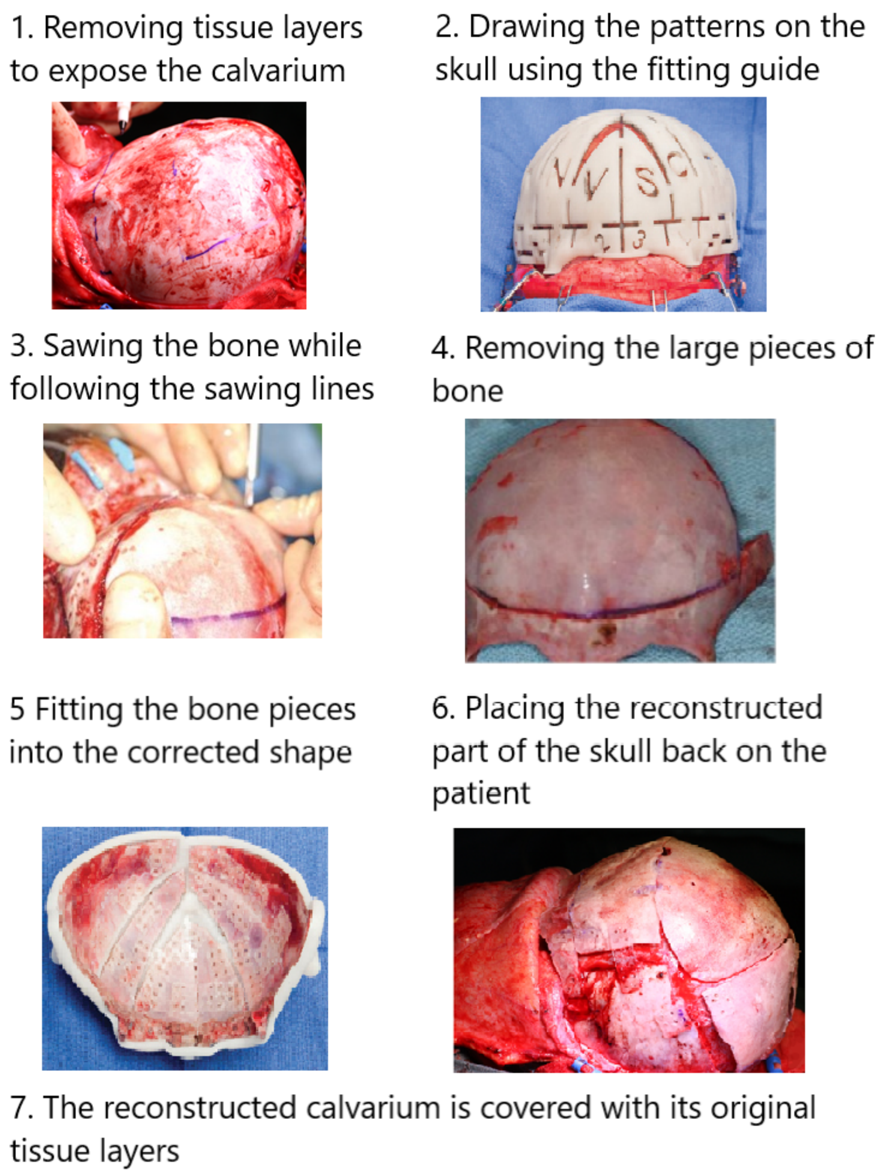

FIGURE 2.1: The intraoperative steps undertaken to recreate the virtual cutting pattern. [6, 15]

Chapter 3

Overview of robotic surgery

3.1 Robotic principles in surgery

Robotic surgery or robotic assisted surgery can be implemented into an operation with various goals. It can provide a higher accuracy, perform certain tasks more efficiently, reduce human errors during certain operating tasks and provide better working conditions for the surgeon resulting in less stress. [16, 17] Robotic surgery requires the robot to monitor both its surroundings (external state) as well as its internal state, which is the relative position of its arms. The internal state of a robot is usually partly planned before a procedure as there are restrictions to the movements of a robot depending on its DOF. The robot can, by partially planning its movements, be avoided to move into configurations in which its movement is restricted. During the operation monitoring of its internal state is done to determine how the robot should move its joints to reach a desired position and orientation. [18]

Monitoring of the external state of a robot can be accomplished using sensors such as optical and electromagnetic tracking to measure and track the distance of the robot to various points of interest or force sensors to monitor the force exerted onto a patient or an object. For the monitoring of its surroundings preoperative imaging is often combined with live information acquired during an operation to gain knowledge about the whereabouts of various anatomical sites of the patient with respect to the robot. Optical tracking is commonly used to acquire live information during an operation. Aligning the coordinate spaces of the preoperative imaging with respect to live positional information is necessary in order to use the preoperatively made scans during the operation. This alignment process of the coordinate spaces is called registration. [19] To perform a registration common points known in both coordinate spaces can be used such as markers placed on a patient or anatomical landmarks. Another way of achieving a registration is by using surface matching.

3.2 Autonomy in robotic surgery

Robotic surgery systems can be classified according to the autonomy given to the robot. Although there is no consensus for the classification of surgical robots, there are a few common classifications for levels of autonomy given to the robot. [19–22] In this chapter an overview of levels of autonomy within robotic surgery is provided and some examples of robotic systems are provided according to the amount of autonomy given to the robot. At the lowest level of autonomy are remote manipulators which are used to enhance the capabilities of the surgeon. These systems leave the autonomy fully to the surgeon. The Da Vinci systems (Intuitive surgical, Sunnyvale United States of America) are a well known examples of these types of robots. Da Vinci systems are used as an alternative to minimally invasive laparoscopic surgery and provide mitigation for some of the human inaccuracies due to tremor and a more ergonomic posture for surgeons in comparison with laparoscopic surgery. [23]

At a higher level of autonomy are passive or semi active systems that position a tool or surgical instrument in the right orientation or provide restriction to the work space of the surgeon, but leave the actual cutting or drilling to the surgeon. [19, 20] An example of a surgical system with this level of autonomy is the Mazor Renaissance. This robot provides an intraoperative guide for the placement of pedicle screws. It uses preoperative CT-scans to make a planning of the desired trajectory and fluoroscopic updates during the operation to provide positional updates of the relative location of robotic device with respect to the patient. [24] Another example would be the robotic interactive orthopaedic arm system (Mako Surgical Corporation, Kalamazoo, Michigan). This robotic system is used to provide haptic and visual feedback to the surgeon during total knee arthroplasty and to restrict the working environment of the surgeon while using the drilling tool. [25]

Intermittent autonomy is a level of autonomy in which the robot performs certain tasks while leaving other tasks to the surgeon. A medical practitioner decides how the task of the robot should be performed. Examples of this level of autonomy that have been used in practice are the Robodoc and CASPAR robots used for total knee replacement. [26–28] There are also a variety of robots under development with an intermittent level of autonomy. Such as a robot for the autonomous placement of sutures for an anostomoses in abdominal surgery, and a robot which can autonomously drill burr holes in maxilofacial surgery. [29, 30] This would be the level of autonomy for our envisioned robotic application if the planning of the sawing lines is still performed by a human.

Another level of autonomy is a situation in which the robot or computer would generate operational strategies from which the surgeon has to select one or give approval for one. The robot subsequently performs this procedure. An example of this level of autonomy used in the clinic is the Neuromate system. This robot performs a trajectory planning for the placement of electrodes which the surgeon has to approve for. Another example is the Cyberknife system which generates a treatment plan based on a preoperative CT scan which the surgeon has to approve. [21, 22, 31] The robot then positions itself in the correct orientation for the radiotherapy while it compensates for the movements of the patient. Another example of a robotic system with this level of autonomy is the Stormram 3 system, which is a autonomous robotic system that can perform a magnetic resonance imaging (MRI) guided needle biopsy's. [32] For its suggested usage an interventional radiologist would have to approve a trajectory before the robot performs the procedure. [16] Yet higher levels of anatomy are to let the robot make surgical decisions without requiring human consent or supervision and to let the robot have full autonomy of a full operation. There are no applications of these two levels of autonomy yet. [20, 21]

Chapter 4

Methods

To develop a robotic workflow for an open cranial vault reconstruction the requirements for a workflow and solutions to these requirements are first determined. This is then used to develop a robotic workflow and implement a simplified version of this workflow within a simulation of this procedure using 3D printed skulls of patients with the craniosynostosis birth deficit. Experiments are subsequently performed to test the error in the implemented workflow and the relative contribution of individual steps of the workflow to the total error.

4.1 Identifying workflow requirements

To determine workflow requirements and suitable solutions to these requirements discussions were held with clinicians and technicians and experience is obtained with participating in the open cranial vault reconstruction in which specific focus was laid on the conveying of the preoperative imaging into the surgical procedure in the current surgical workflow. Also a literature search was performed focusing on optical tracking, current implementations of workflows for surgical robotics, their registration methodology and general registration strategies. The following requirements were determined for the robotic workflow:

- The robot to be used has to be mobile so that surgeons can perform certain procedures and the robot others.
- For the robot to perform either the drawing of the sawing lines or saw these drawing lines it would be essential that the skull of the patient is detected and traced by a 3D tracking system.
- It would also be essential that the frame of the tracking system (F_c) can be accurately aligned with the base frame of the robot (F_0). This alignment procedure has to occur in a way in which it does not have a large impact on the workflow of the surgery.
- After a successful alignment the tracking system has to be able to detect patient movements with a reaction speed equal to or better than the reaction speed of a surgeon.
- Adequate line of sight of the tracking system on the patient must be maintained during the robotic procedure.
- A robotic sawing procedure guided by a tracking system would be subjected to the following sources of inaccuracies: a skull detection error, a frame alignment error (for aligning F_c to F_0), the error of the robot, and an error which occurs during the tracing of the pose of the patient. It is not clear at what deviation compared to the planned pattern, the sawed pattern becomes functionally worse at creating space

for the brain to develop or at what deviation from the planned pattern the sawed pattern would have a clearly noticeable aesthetic impact. This is of course highly dependent on the cranial shape of the patient and the created virtual planning. In the current practice deviations of 1.5 mm are expected to occur due to slightly incorrect guide placements, drawing inaccuracies and sawing inaccuracies. With the existing clinical practice of using a surgical guide, the patterns can be drawn on a 3D printed skull with a mean Euclidean error of 0.9 mm and a standard deviation (SD) of 0.6 mm compared to the actual planned pattern. [11] With these considerations and error measurements in mind an application is deemed to be clinically relevant if a robot is able to mark the preoperative planning with a mean Euclidean error of less than 1.5 mm.

Solutions to these requirements were determined based on the practicality of the solution, the effectiveness found in the literature and how well a solution would fit with the requirements of the workflow.

4.2 Developing & implementing the robotic workflow

The surgical workflow for performing a robotically assisted open vault crainial reconstruction is subsequently developed. Arguably the least difficult step for a robotic implementation would be to instruct a robot to draw preoperatively determined sawing patterns on the skull of the patient, since the drawing itself is a non-invasive procedure that requires no sawing in bone as the other steps do. This part of the surgical procedure can also be expanded into more invasive robotic tasks when it is implemented and it is practical for error testing as the 3D printed skulls can be used multiple times. This is therefore chosen to be the first step for implementing this robot in the surgical procedure. To describe how the workflow is developed and implemented a overview of the system is given and each part of the workflow is subsequently described.

4.2.1 System overview

Components of the robotic system

The composed robotic system which is used for the workflow consists of the following components:

- The PST base HD tracking system, which is used to locate the position and orientation of objects, such as the 3D printed skulls.
- A laptop to process the signals coming from the stereo camera, perform calculations to align the incoming poses in the frame of the camera F_c with the frame of the robot base F_0, and send positions and orientations of objects to the robot.
- An Omron Viper 850 robot, which is controlled via the MotionBlox-60R controller.
- The ACE software platform, which provides a way of sending scripts and commands from the laptop to the robot and can receive messages from the robot.

Connecting the components

The robotic controller can receive data from the laptop, such as the tracking data from the stereo camera, by means of an ethernet connection and with the help of a script composed using the ACE software. The PST base HD is connected to the laptop by USB. Tracking

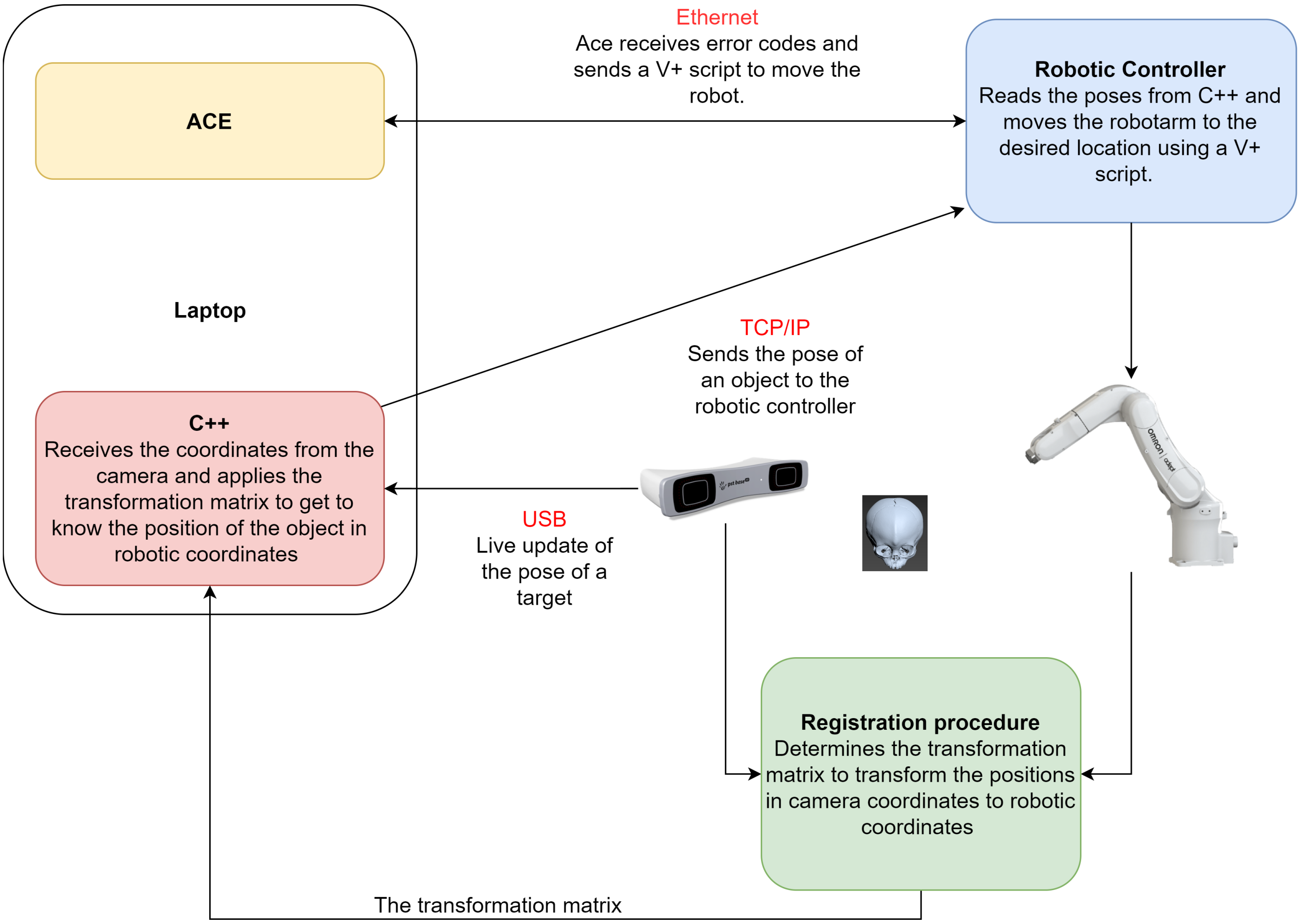

FIGURE 4.1: The entire robotic system and the method with which coordinates are received, processed and sent to the robotic controller.

information can be acquired from the cameras using the software development toolkit (SDK) of the PST camera, which is written in C++. This SDK is used to output the live position and orientation of objects detected by the PST stereo camera in C++ as transformation matrices. A registration procedure described in section 4.2.3 is used to find the $\mathbf{H}_0^C$ transformation matrix used to convert poses expressed in F_c to poses expressed in F_0. After this transformation is applied, poses of the target in robotic coordinates can be send to the robotic controller using the transmission control protocol / internet protocol (TCP/IP). The entire robotic system and its way of receiving information detected by the stereo camera is shown in figure 4.1.

Trajectory planning

In order to perform a robotic procedure with respect to a patient, a scan of the patient needs to be available to define the desired trajectory of the robot respect to this patient. In the case of craniosynostosis surgery the trajectory of the robot can be defined with respect to a reconstruction of the skull from a CT scan of the patient. The reconstruction of the skull from the CT scan can be matched to the actual skull when the skull is detected during a surgical procedure. In this thesis three scans of patients with craniosynostosis are 3D printed and used as a substitution for actual skulls. In section 4.4 it is described how a virtual planning with respect to these 3D printed skulls is made and how the tracking system detects these 3D printed skulls. When the virtual planning is registered to the pose of the 3D printed skull detected with the tracking system and when the frame of the tracking system is registered to the frame of the robot the trajectory defined in the virtual planning can be followed with the robot. The robot only uses Euler angles in the 'ZYZ' convention to specify the orientation of its flange with respect to its base frame. The desired poses to which the robot has to move to are therefore converted to 'ZYZ' Euler angles prior to sending them to the robot. The flange of a robotic arm is the surface on the most distal end of arm onto which tools can be attached.

4.2.2 Object detection

Optical tracking systems, such as the PST base HD used in thesis, use information acquired from two or more cameras to determine the position of objects in a measurement volume. To detect objects the PST base HD tracking system emits near infrared light. This light is reflected by reflective markers and spheres placed on top of a target object. The reflections of the target objects are detected by the two image sensors located inside the PST base HD tracking system and are internally processed to produce 3D coordinates of the centers of these reflective markers and spheres. In order to accurately determine the positions of objects a calibration procedure is required. In this procedure the intrinsic and extrinsic parameters of the stereo cameras are determined. [33] These parameters are the pose of the two cameras, the focal distance, optical center, and lens distortion coefficients. [34] The calibration of this tracking system is performed by PS tech. To detect a model the positions of the markers relative to a self defined local origin are supplied as input to the camera system. The camera can recognize the marker configuration and give the pose of the local origin of the detected model. [35]

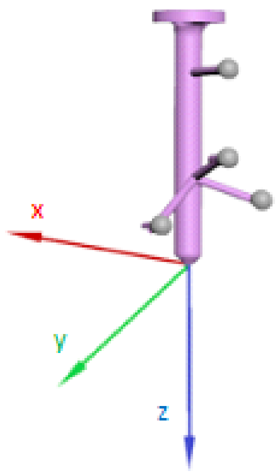

FIGURE 4.2: The pointer with its defined local frame.

4.2.3 Registration

In order to register the camera frame to the base frame of the robot a pointer is designed which can be traced by the PST base HD system. The origin this pointer is located at the tip of the pointer. Its z-axis is defined to be running along the axis of the pointer from its base to the tip, the x- and y-axis are arbitrarily selected and are perpendicular to the z-axis. The pointer and its frame is displayed in figure 4.2. On this pointer four reflective spheres are attached. Their position with respect to the origin of the frame is determined by making a cone beam computed tomography (CBCT) scan of the pointer. The positions of centers of the spheres are supplied to the PST base HD tracking system.

The pointer is attached to the middle of the robot flange so that the pose of the tool expressed in the base frame of the robot can be determined by knowing the pose of the robot flange and the height of the pointer. The pointer is 3D printed so that its height is determined beforehand. The acquired CBCT scan is used to validate the accuracy of the 3D print. The flange pose with respect to the base frame of the robot $\mathbf{H}_0^F$ is calculated by the robotic controller using the servomotors of each joint.

For the registration procedure the pointer is moved to 5 predetermined poses in which the tip of the pointer is located in the outskirts of the workspace of the robotic application as recommended in [36]. The workspace with an example of a skull reconstructed from a CT scan is illustrated in figure 4.3. The position of the tip of the tool is determined by using the flange pose given in Euler angles and the xyz-coordinates of the flange. To convert the poses of the flange to poses of the pointer the following formula is used $\mathbf{H}_0^F = \mathbf{H}_{PT}^F \mathbf{H}_0^{PT}$. While the robot follows a trajectory to the 5 predetermined poses, the pose of the pointer can be tracked using the PST HD base system. The tip positions at these 5 predetermined locations measured by the tracking system can then be registered to the tip positions measured with the robot by means of the Procrustes algorithm to produce the $\mathbf{H}_C^0$ transformation matrix. The fiducial registration error is used as an error metric to check for a correct alignment of the points. We can apply the found transformation to every object detected by the tracking system to obtain its position in the base frame of the robot.

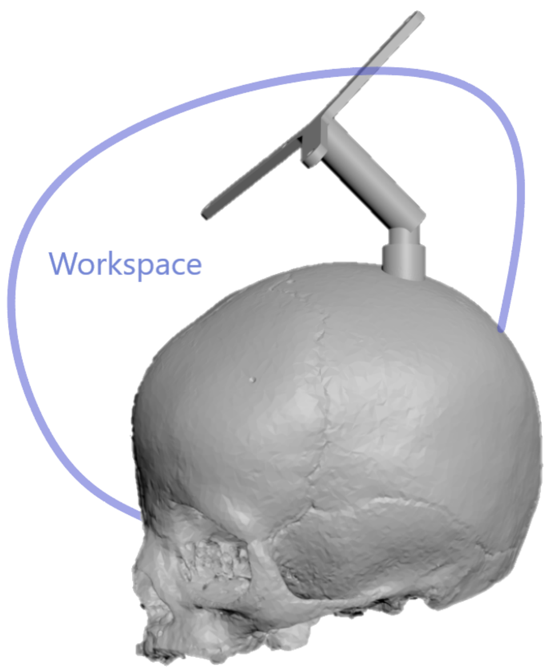

FIGURE 4.3: The workspace of the robotic application with respect to a 3D printed skull.

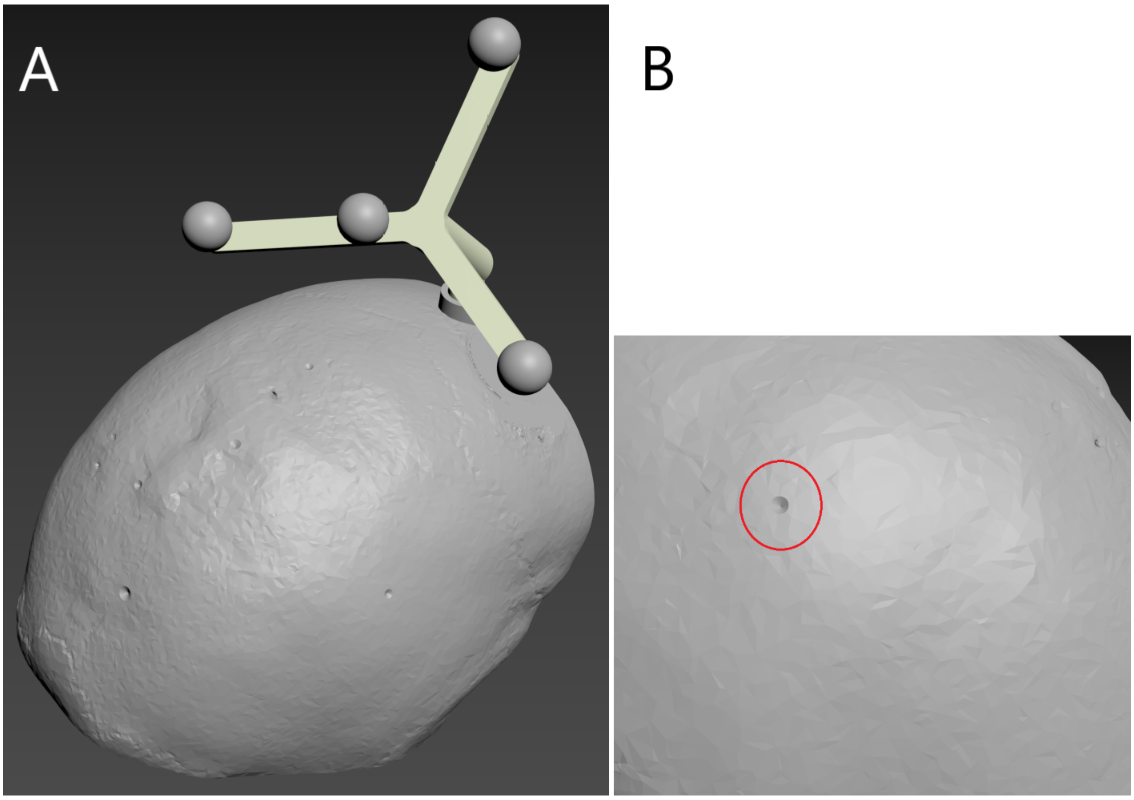

FIGURE 4.4: A skull reconstructed from a CT scan with the reference star attached is shown in A. B shows a cone shaped notch encircled in red.

4.2.4 Defining robotic movements

To implement this workflow into a simplified version of a simulated robotic workflow during an open cranial vault remodeling three 3D printed skulls are used. The three 3D printed skulls are made out of CT scans (with a slice thickness of 0.5 mm, and a slice increment of 0.5 mm) of patients with the craniosynostosis birth deficit. The patients were operated with the help of a preoperative virtual 3D planning and they received a CT scan as part of the standard preoperative workflow. 3DmedX software (v. 2.1, 3D lab RadboudUMC, Nijmegen, The Netherlands) is used to create 3D models of the patient's calvaria using threshold based segmentation.[11] An attachment mechanism is made onto each skull and small cone shaped notches are made at the intersections and corners of the sawing lines of the preoperative planning. The models are 3D printed using selective laser sintering. An attachable object containing four reflective spheres, which shall be called reference star from now on, is made to enable the detection of the model with the help of the 3D camera. This is thus a simplification from the markerless detection and tracking that would be required to make this workflow feasible for implementation within an actual open cranial vault reconstruction. The reference star attached to a skull is depicted in figure 4.4A, figure 4.4B shows a cone shape notch made on the skull.

CT and CBCT scans of the 3D printed skull with the reference star attached are acquired to find the positions of the reflective markers with respect to the 3D printed skull. A virtual target location is set on each of the small notches on these CT and CBCT scans using 3DS max software (Autodesk, Mill Valley, United States of America). These locations are targets for the robotic arm. The target orientation of the robot tool is set to be in the inverse direction of the normal of the scanned outer surface of these CT scans. The desired poses of the pointer with respect to the frame of the scanned object ($\mathbf{H}_P^D$) are determined. The frame of the scanned skull is called the planning frame.

4.2.5 Workflow for implementation

The workflow in which the tracking system and robotic system are connected with oneanother is build in the form of 2 custom build programs. One program which performs the required registration (and can be performed without the 3D printed skull present) in preparation of the robotic movements to the skull, and the other program which performs the actual movements using the information provided by the first program and a detected 3D printed skull. The programs are build using C++ to enable an efficient interaction with the tracking system and to create an efficient architecture in which coordinates can be exchanged between the robot and the tracking system. This architecture allows for movement compensation based on the tracking information acquired by the PST base HD system. Each of the C++ programs is paired with a program in the V+ programming language (Omron, Kyoto, Japan) which is composed using ACE and send to the robotic controller.

An important objective for this thesis was to make sure that there is no bug in the implemented programs. This is important for the determination of the error of the implemented workflow and to figure out which parts can be improved. For debugging this application a virtual simulation is build in Matlab (version 2020a, MathWorks, Natick, USA). In this virtual simulation the mathematical operations of the C++ programs are performed in the same order. This virtual simulations is build to first of all check for errors in the manually written functions such as the Procrustes algorithm in 3D and the conversion of rotation matrices into Euler angles. It is also build to input simplified translation and rotation values into all mathematical operations of the workflow to check for errors. It was apart from that used to visualize (simplified) output of functions and the successive transformations performed in the workflow.

4.3 Validation of total workflow

An experiment to validate the workflow is performed. The robot end effector is in this experiment moved to the target poses defined with respect to the 3D printed skulls using the developed programs described in section 4.2.5 and 5.2.1. This is done three times using three different registration trajectories in the preparation stage of the workflow. These registration trajectories are all performed with the same goal, achieving registration, but different poses are selected for each of the 3 registration trajectories to receive preliminary information on the influence of selecting different poses in the registration procedure. The poses used in the registration trajectory are selected to have their tip position in the work space of the surgical procedure as described in section 4.2.3.

The used 3D printed skulls contain 4 target points for the patient with plagiocephaly, 5 target points for the skull of the patient with trigonocephaly and 6 target points for the skull of the patient with scaphocephaly. After each followed registration trajectory the surgery stage of the robotic program is performed in which the end effector of the robot is programmed to move to the desired pose defined on each 3D printed skull. The target locations are the notches created on the 3D printed skull. Patients with different pathological skull shapes are selected in order to create a simulation which closely resembles the movements that an implemented robotic system would have to perform on patients in a simplified fashion. The 3D printed skulls with reference star attached are placed at a distance of 55 ($\pm$3) cm from the origin of the robotic base frame in the direction of the negative y axis of the base frame of the robot as depicted in figure 4.7A. The reference star is in every measurement directed to the stereo camera as also illustrated in figure 4.7. The tracking system is placed 17 cm ($\pm$3 cm) away from origin of the skull in the z direction of the robotic base frame and 36 cm ($\pm$3 cm) away from the skull in the x direction. The tracking system is angled with a pitch of 20° with respect to the base frame of the robot. In this experiment the robot marks 15 target points on three 3D printed skulls of patients for each registration trajectory.

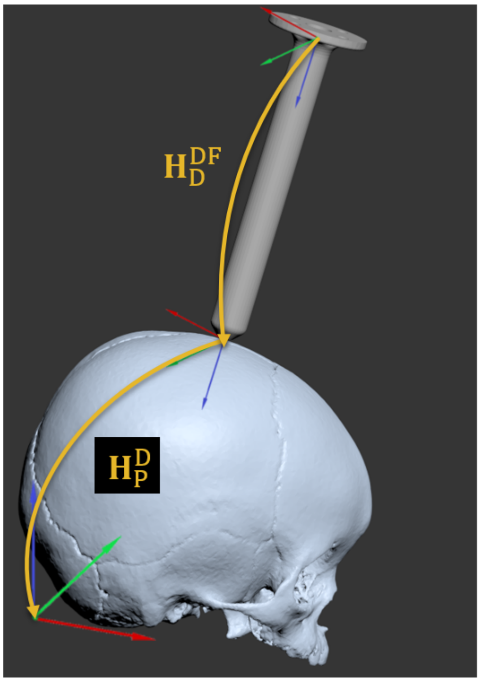

FIGURE 4.5: An example of a desired pointer pose defined with respect to the frame of the planning by the $\mathbf{H}_P^D$ transformation matrix. The $\mathbf{H}_D^{DF}$ which describes the desired pose of the tool with respect to the robotic baseframe is shown as well.

For this experiment a pen with at its base a spring is inserted in the 3D printed pointer as shown in figure 4.8. This mechanism with a spring is selected for two reasons. The first reason is that in a later stage a force sensor will be added to ensure a sufficient accuracy for the direction perpendicular to the surface. The accuracy in the working direction of the spring is thus less relevant for a future application. The spring is also added to mark a 3D printed skull without damaging neither the skull nor the pen.

For the marking of the pattern on the 3D printed skull the robot is programmed to first move to a generic home pose that can be described with the $\mathbf{H}_0^{\mathrm{Home}}$ transformation matrix. This home pose defined in the robotic base frame is located at a 0.4 m displacement in the direction of the z-axis from the center of the 3D printed skulls. The orientation of this pose is with its z axis directed at the negative z-axis of the base frame of the robot and its x and y axis parallel to the x and y axis of the robotic base frame. The home pose is shown in figure 4.7. The robot is programmed to move its flange to the desired pose after this home pose is reached, in which it approaches this pose from the negative z-axis of the desired pose. An example of a desired pointer pose is depicted in figure4.5. The described trajectory is made to avoid collisions with the skull while approaching the targets on the skull. The distance from the patterns drawn on the 3D printed skull to the associated notches are determined using a digital caliper (Mitutoyo, Kawasaki, Japan). The mean and SD of the Euclidean distance is calculated for each registration trajectory. The performed measurements are summarized in figure 4.6.

	Scafocephaly	**Plagiocephaly**	**Trigonocephaly**	**Total (per registration movement)**
Registration trajectory 1	5	4	6	15
Registration trajectory 2	5	4	6	15
Registration trajectory 3	5	4	6	15
Total (per 3D printed skull)	15	12	18	45

FIGURE 4.6: Amount of measurements done on the 3D printed skulls.

4.4 Validation of camera and robot separately

In a second experiment the stereo camera and robot is validated separately. This is done to determine the relative contribution of each component of the workflow to the total error in the workflow. In this experiment mm paper is used, which is placed in between 2 plates of glass of 2mm in thickness to ensure that the paper is even and flat. Four target points are selected on the mm paper in a square. The plates are angled with a pitch of $0°$ ($\pm 3°$) and $25°$ ($\pm 3°$) with respect to the xy plane of the base frame of the robot. Half of the experiments are performed with the plates of glass angled at a pitch of $0°$ ($\pm 3°$) and the other half with the plates of glass angled with a pitch of $25°$ ($\pm 3°$).

The robot is manually moved to the four locations. To ensure that the pointer tip reaches the predetermined location, it is checked if the tip of the pointer lies in between the two adjacent lines on the mm paper. This is done for both directions of the mm paper. The location of the tip of the pointer at the four predefined target points is determined by the robotic system and by the PST base HD. The PST base HD is angled with a pitch of $20°(\pm 3°)$ with respect to the base frame of the robot. The distance of the tracking system to the center of the four points is 20 cm (± 3) in the z direction and 45 cm (± 3) in the x direction of the robotic base frame. The scene is depicted in figure 4.7B.

In one set of measurements the pointer is brought to the four points on the mm paper with its z-axis always orientated orthogonal to the plates of glass and in the second session its orientation is varied. The variations in the orientation have the following constraints expressed as an intrinsic rotations in Euler angles in the XYZ representation and

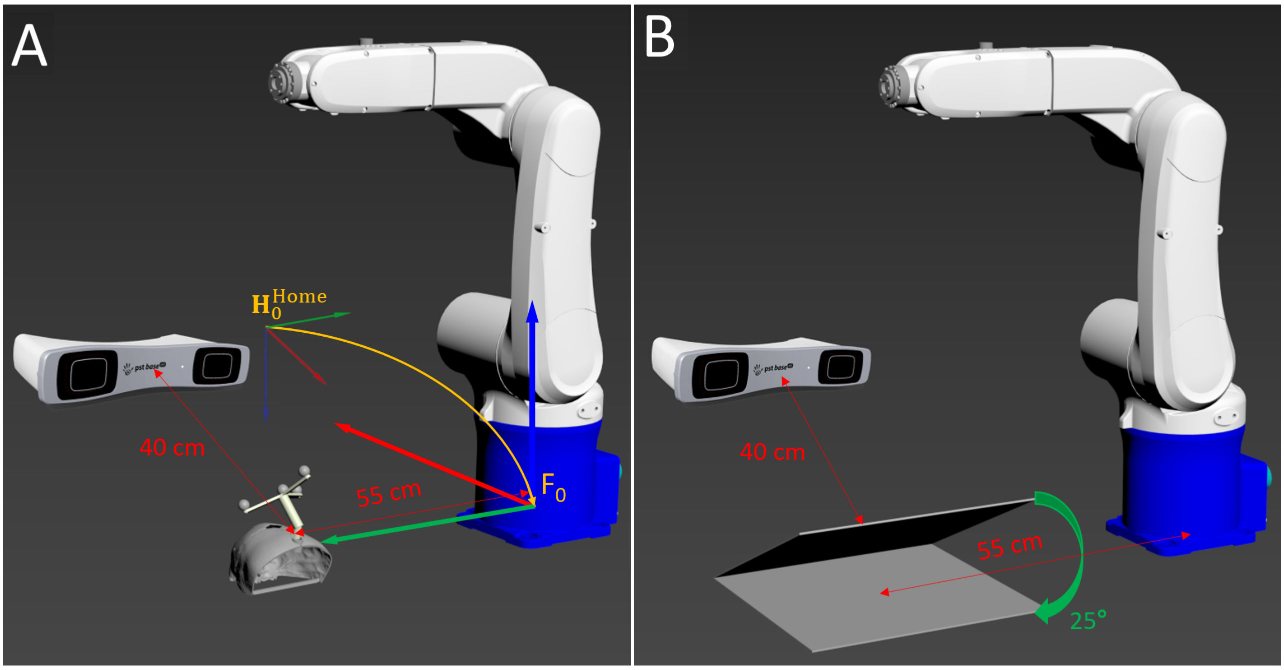

FIGURE 4.7: A scematic virtual scene of the experiments. Scene A depicts the workflow experiment. Scene B depicts the experiment in which the accuracy of the workflow is tested with mm paper between plates of glass under a pitch angle of 25°and 0°with respect to the base frame of the robot. The $\mathbf{H}_0^{Home}$ transformation matrix which expresses the home pose with respect to the base frame of the robot is also depicted as well as the robotic base frame F_0.

FIGURE 4.8: Spring inside a generic pointer. [37]

with respect to the base frame of the robot: [80°< pitch < 230°] , [-45°< yaw < 15°] , [-10°< roll < -210°]. In each set of measurements the distance between adjacent points is determined with the tracking system, the robot and the mm paper. The total experiment is repeated 2 times. This results in a total of 16 measurements in which the orientation with respect to the plate of glass is varied and 16 measurements in which the orientation is remained constant. The difference between the distance determined with mm paper and the distance measured by means of the tracking system is calculated, and the difference between the distance determined with mm paper and with the robot is calculated. The mean absolute error and the SD of the absolute error of these determined differences is calculated for the measurements in which the orientation in varied and for the measurements in which the orientation is kept constant. These error metrics are selected because they provide a high amount of interpretability to the found error.

Chapter 5

Results

5.1 Robotic workflow

A workflow is developed for implementing a robotic system within an open vault reconstruction for craniosynostosis. Based on the determined requirements the workflow is setup in the following way. A camera setup is used which is not attached to the robot but positioned externally to be able to stably direct the camera to the patient throughout the procedure. The alignment of the robotic frame to the frame of the tracking system is done during a registration in the preparation stage to minimize the influence of this registration procedure on the workflow of surgery. During the surgery stage the tracking system is used to track the skull of the patient and to provide feedback for the movements of the robotic system. The information acquired during the preparation stage is used to transform the acquired skull pose found by the tracking system to the robotic base frame in the surgery stage. To eventually allow for movement compensation, the interaction between the systems is setup in the most direct manner to efficiently receive and process the send patient pose. The designed workflow is shown in figure 5.1.

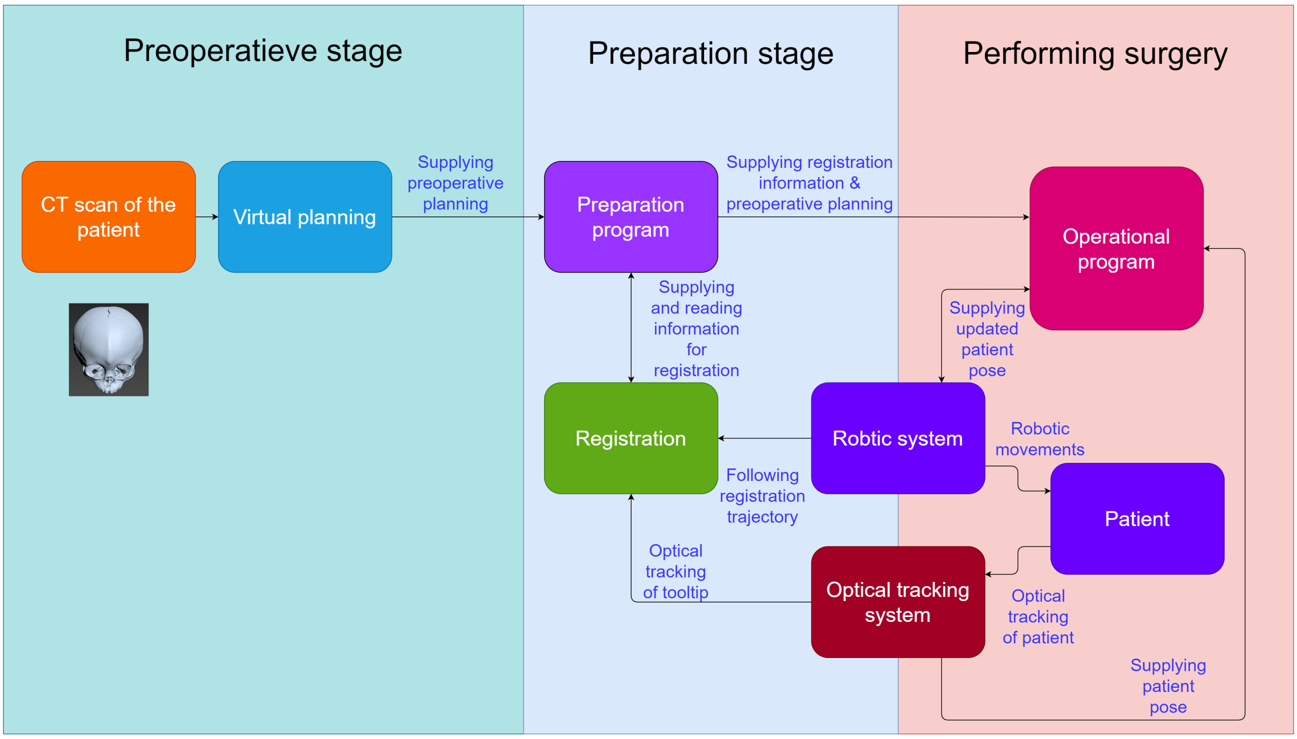

FIGURE 5.1: The developed workflow for implementing robotic surgery into a open cranial vault reconstruction for craniosynostosis.

5.1.1 Implemented workflow

This developed workflow is implemented in the following way in a simplified version of the robotic movements that would have to be performed during a robotically assisted open vault reconstruction:

Preparation stage

The following operations are performed during the preparation stage (presence of skull is not required):

1. Load the 5 predefined pointer poses expressed in the baseframe of the robot $\mathbf{H}_0^{PT}$ into the program.

2. Transforming the pointer poses in the robotic base frame to flange poses in the robotic baseframe $\mathbf{H}_0^F = \mathbf{H}_{PT}^F \mathbf{H}_0^{PT}$. The $\mathbf{H}_{PT}^F$ matrix in this formula is the homogeneous transformation matrix used to convert poses in the frame of the pointer to poses expressed in the frame of the robot flange.

3. Start the tracking of the pose of the pointer and storing the position of the origin of the pointer (which is equivalent to the tip of the model) in collection ${}^c\mathbf{p}_{\text{origin}}(i)$ with $i = \{1, 2, 3 .. n\}$ in which i is the current iteration of the gathered data and n the total amount of iterations.

4. Ordering the robot to move its end effector to the 5 flange poses $\mathbf{H}_0^F$. This is done by sending the 5 flange poses to the robot using a TCP/IP connection, with the laptop as server and the robot as client, and initiating the robotic V+ program in which the connection to the server is established, the poses are subsequently read and the robot is commanded to move to the 5 poses in a specified time interval.

5. Automatically identifying the iterations in the recorded tracking data at which the robot reaches a target pose and at which the robot moves away from a target based on the duration of each robotic movement. This results in the following 2 vectors: $\mathbf{xb} = \{\mathrm{i}_{1b}, \mathrm{i}_{2b}, \mathrm{i}_{3b}, \mathrm{i}_{4b}, \mathrm{i}_{5b}\}$, $\mathbf{xe} = \{\mathrm{i}_{1e}, \mathrm{i}_{2e}, \mathrm{i}_{3e}, \mathrm{i}_{4e}, \mathrm{i}_{5e}\}$.

   In which **xb** contains the iterations at which the robot arrives at a target point and **xe** contains the iterations at which the robot moves away from a target point. This is done in order to find the recorded iterations at which the pointer is positioned at a target pose.

6. Determining the average tooltip position measured with the camera at each target pose in the camera frame F_c.

   for k = 1 to 5

   $$ {}^c\mathbf{p}_{\text{target}}(\mathrm{k}) = \sum_{\mathrm{i}=\mathbf{xb}(\mathrm{k})}^{\mathbf{xe}(\mathrm{k})} \frac{{}^c\mathbf{p}_{\text{origin}}(\mathrm{i})}{\mathbf{xe}(\mathrm{k}) - \mathbf{xb}(\mathrm{k})} $$

7. Extracting the pointer tip positions in the robot base frame ${}^0\mathbf{p}_{\text{target}}$ from the $\mathbf{H}_0^{PT}$ transformation matrix.

8. Using the Procrustes algorithm to register the camera frame F_c to the robotic base frame F_0 by aligning ${}^c\mathbf{p}_{\text{target}}$ to ${}^0\mathbf{p}_{\text{target}}$. [38] From this procedure the $\mathbf{H}_0^c$ transformation matrix is constructed.

9. Calculating the Fiducial Registration Error (FRE) to check for an accurate alignment of ${}^c\mathbf{p}_{\text{target}}$ to ${}^0\mathbf{p}_{\text{target}}$.

Operation stage

These operations are performed to move the tool to desired poses defined on a CT scan of the 3D printed skull on which target locations are defined:

1. Defining the $\mathbf{H}_D^{DF}$ and $\mathbf{H}_P^{D}$ transformation matrices. The $\mathbf{H}_D^{DF}$ transformation matrix describes the desired pose of the flange with respect to the desired pose of the pointer. The $\mathbf{H}_P^{D}$ transformation matrix describes the desired pose of the tool with respect to the robotic base frame. An example of a desired pointer and flange pose is shown in figure 4.5.

2. The $\mathbf{H}_0^{C}$ transformation matrix is read from the output of the first program.

3. Setting up a TCP/IP server from the laptop and executing the associated robotic program to make a connection from the laptop with the robot.

4. The tracking system supplies the pose of the 3D printed skull with respect to the camera frame in the form of the $\mathbf{H}_C^{P}$ transformation matrix to the program upon detection of the reference star attached to the 3D printed skull.

5. The desired flange poses are converted to base frame coordinates using the following formula: $\mathbf{H}_0^{DF} = \mathbf{H}_0^{C}\mathbf{H}_C^{P}\mathbf{H}_P^{D}\mathbf{H}_D^{DF}$.

6. The desired flange pose in the robotic base frame is converted to Euler angles in the 'ZYZ' convention.

7. The flange pose defined in Euler angles is sent to the robotic controller.

8. The program on the robotic controller reads the pose data and performs the planned movements in which the robot moves its flange to the target pose.

5.2 Validation of implemented workflow

The workflow validation experiment indicated that with this implementation successful connections can be made with the different components of this workflow. The validation experiment resulted in a mean Eucludian error of 3.9 mm ($\pm$ 0.79 SD), 4.0 mm ($\pm$ 1.1 SD) and 3.9 mm ($\pm$ 0.78 SD) for reaching the desired targets on the skull after each of the performed registration movements. The results of the workflow validation experiment is depicted in figure 5.2.

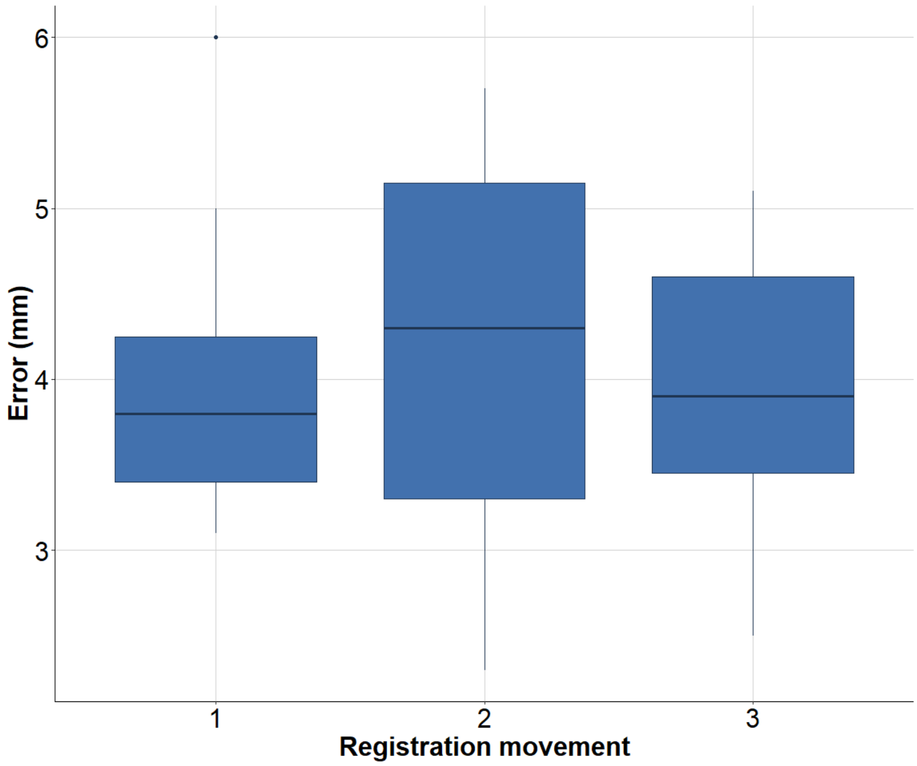

FIGURE 5.2: The Euclidean distance of the marking set by the robot with respect to the to the associated notches on the 3D printed skulls.

5.3 Validation of the stereo camera and robot separately

5.3.1 Stereo camera

For the validation experiment of the stereo camera a mean absolute error of the measured distance with the stereo camera with respect to the distance determined with mm paper is 0.52 mm (±0.33 SD) for the measurement in which the angle of the pointer with respect to the plateau is remained constant. The mean absolute error is 0.72 mm (±0.48 SD) for the measurements in which the the pointer orientation with respect to the plane is varied.

5.3.2 Robot

For the validation experiment of the robot a mean absolute error of the measured distance with the robot with respect to the distance determined with mm paper is 0.59 mm (±0.38 SD) for the measurement in which the angle of the pointer with respect to the plateau is remained constant. The mean absolute error is 1.6 mm (±1.3 SD) for the measurements in which the the pointer orientation with respect to the plane is varied. A boxblot of the absolute values of errors is plotted in 5.3.

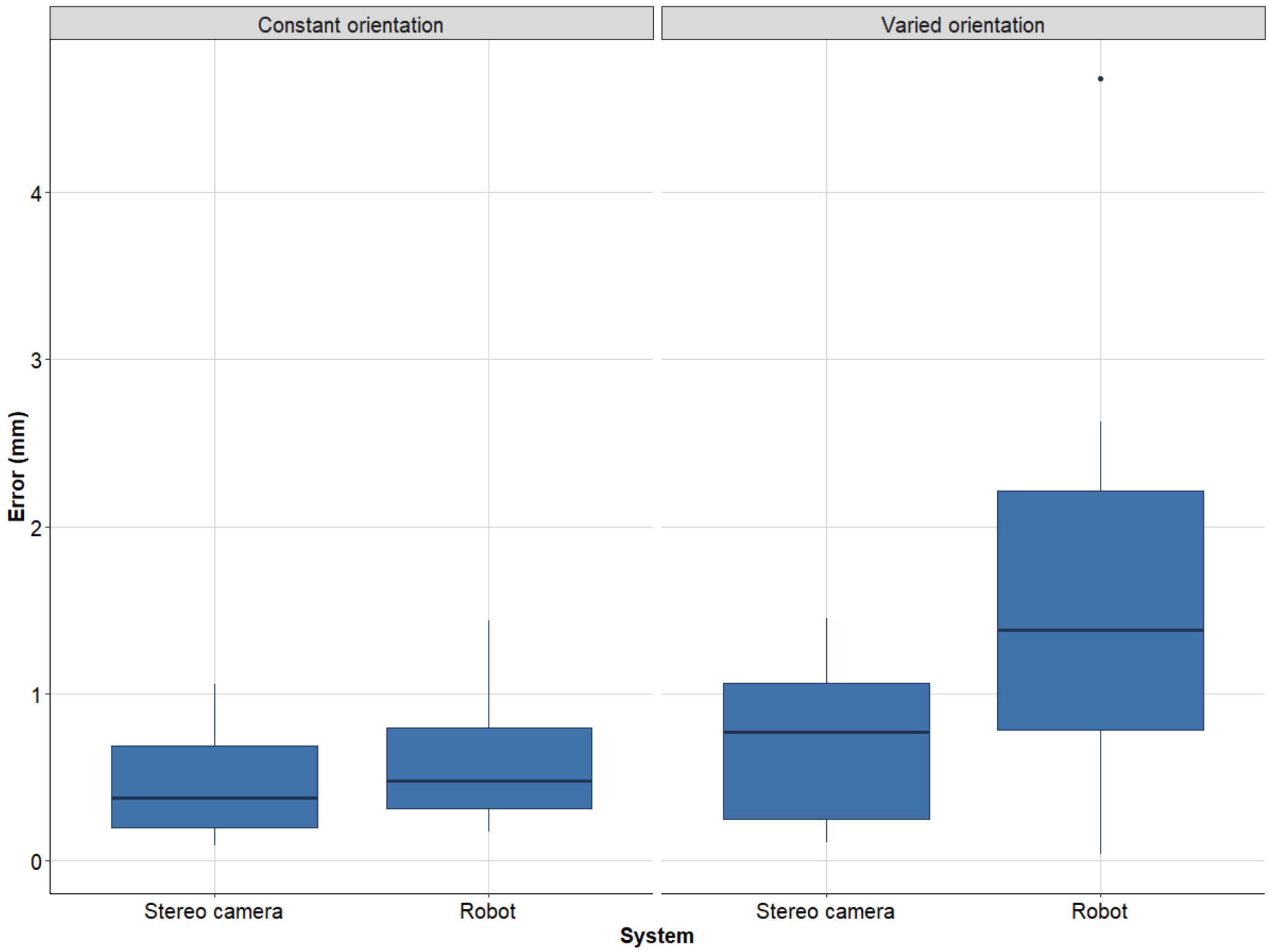

FIGURE 5.3: Boxplot of the absolute error of the measurements done on mm paper.

Chapter 6

Discussion

The goal of this thesis was to setup a workflow for the implementation of a robotic system in open cranial vault remodeling and to test the validity of an implementation of this workflow in a simulated and simplified procedure. With the designed workflow the procedure can be separated in a preparation stage which can be performed before the presence of the patient and a stage in which the surgery is performed. Performing a registration of the tracking system to the robotic base frame in a preparation stage and implementing direct communications of the laptop with the stereo camera and robot as presented in this workflow fits with the requirement of achieving a robotic workflow that is efficient with regards to to the surgical operating time and that has the ability to perform movement compensation. The found mean Euclidean error of 3.9 mm ($\pm$ 0.79 mm SD), 4.0 mm ($\pm$ 1.1 mm SD) and 3.9 ($\pm$ 0.78 mm SD) for three distinct registration trajectories makes the implementation of this workflow in its current form and with the currently used materials not accurate and precise enough for a clinical implementation. The inaccuracy of the Omron Viper 850 industrial robot in determining its flange pose with respect to its base frame seems to be the largest source of the error in the workflow. Using a robot in which the internal parameters are known with a higher accuracy, and using a more suitable stereo camera system for the surgical procedure are recommended to lower the error in the workflow.

6.1 Explanation of the results

6.1.1 Solutions workflow requirements

Stereo camera setup

As a solution for the requirement of patient tracking it was opted to use an external stereo camera system for the tracking of the pose of the skull. A stereo camera system can also be attached to the robot. An advantage of such a setup is that the robot can approach the target from different angles to better register the pose of the patient with respect to the camera. A disadvantage of such a setup would however be that the camera has vision of different parts of the skull at different times during the operation. When the robot is for example sawing patterns at one side of the skull the other half is not seen by the robot. It would because of this constantly changing perspective be far more challenging to accurately track the movements of the skull of the patient during the operation.

Force sensor

For the robot to autonomously saw according to the predetermined pattern the accuracy of a 3D camera and CT scan (voxel size = 0,5 mm x 0,5 mm x 0,5 mm, Aquilion One, Toshiba, Tochigi, Japan) might not be sufficient to ensure that the robot does not inflict any tissue damage. [39] A Force sensor can provide extra reliability in preventing tissue damage by providing feedback on the amount of force exerted on the tool in multiple directions. During a motion the force exerted in a particular direction of the tool can be constrained by sending positional feedback to the robot based on the force exerted on the tool in this direction. [40] If the planned orientation of the tool remains perpendicular to the surface of the skull during a robotic movement a force sensor can measure the force in the z direction of the tool to prevent the tool from inflicting tissue damage during this movement as illustrated in figure 6.1. Force sensors have been applied to a variety of surgical robots in experimental setups and clinical practice and these sensors are able to provide sufficiently accurate readings of the force and torque applied to a robotic tool to prevent a tool from damaging soft tissue. [40, 41] Implementation of a force sensor to achieve a higher accuracy during the operation might be necessary for eventually autonomously performing the surgical operation.

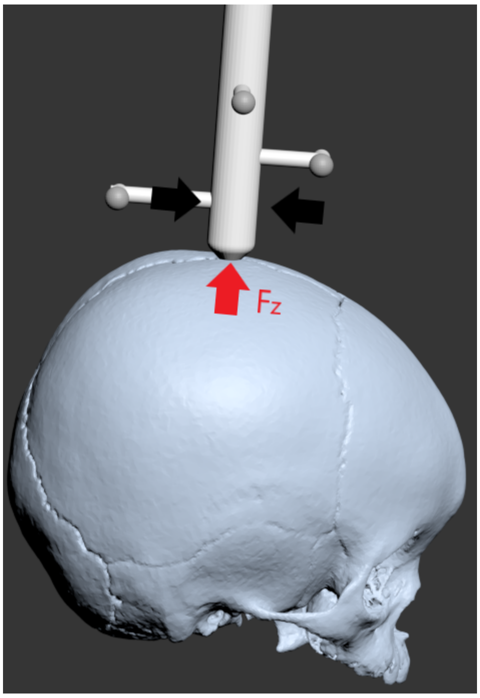

FIGURE 6.1: A skull with a pointer is shown. Examples of measurable forces on the pointer are indicated by black and red arrows. The most relevant force in this situation is F_z, indicated in red. Positional errors and thus a high exerted force is the most relevant in this direction as too high forces in this direction will likely result in tissue damage. High forces in the other directions are more likely to be intentional during a sawing movement and are expected to be less likely to result in tissue damage.

6.1.2 Developed robotic workflow

In the developed workflow the registration of the camera frame to the robotic frame can be performed before the presence of the patient. The surgical operating time can in this way be reduced compared to a registration procedure that has to occur during the surgical procedure. This is suitable treat for an open skull reconstruction considering that a longer operating time leads to more blood loss. The error in this workflow is however too high for a clinical implementation. The error resulting from the experiments on the entire workflow can be subdivided in the following 5 factors:

1. The accuracy in finding the positions of the spheres on the 3D printed models by using their CT and CBCT scans.
2. The accuracy in defining the target points on the virtual skull with respect to the actual locations of these targets on the 3D printed skull.
3. The error in the localization of models using the PST base HD system
4. The error of the Procrustes algorithm.
5. The accuracy of the robot in determining its flange pose with respect to its base frame.

Some sources of errors occur multiple times in a slightly different fashion during the workflow such as the detection of a pointer during the registration procedure and the detection of a 3D printed skull during the marking of a preoperativelly determined pattern. Or the movements of the robot during the registration procedure and during the marking of the target. For most of these errors an estimation of its contribution to the total accuracy and precision can be made. The precision in a set of measurement is the spread between the points. The accuracy is the distance of these points to a predefined target.

Error due to CT and CBCT scans

The voxel sizes of the CT and CBCT scans are 0.6 mm and 0.2 mm respectively so it can be assumed that the maximum error of finding the reference spheres on the used models is equal to or less than 0.6 mm. The error with which the target points on a virtual model can be defined compared to the physical version of that model is also dependent on the accuracy of the CT and CBCT scans of that 3D printed skull. The contribution of this error to the error of the entire workflow is therefore also expected to be lower then 0.6 mm. These sources of errors result in an inaccurate registration since each tip position is in actuality located at a different location due to an error in the localization of spheres on the pointer. The error in finding the relative location of the spheres on the reference star also causes an inaccurate result as the pose of these models will be misplaced due to an inaccurate localization of these spheres.

Error caused by the CT scan and stereo camera system combined

The experiment in which the stereo camera is used to measure the position of the tip of the tool while moving it to four predefined points on mm paper sheds light on the combined error of finding the location of the spheres in the frame of the CBCT scan, determining the relative position of the reflective markers on the pointer in the camera frame with the tracking system, and acquiring the position of the tip of the pointer based on the pointer pose determined by this tracking system. The measurement in which the pointer pose is varied is especially helpful for determining the contributions of these sources of error to the total error of the workflow, since this experiment more closely resembles the movements performed during the workflow. Based on this measurement, which reports a mean absolute error of 0.72 mm ($\pm$0.48 SD) the conclusion can be made that the relatively poor accuracy found in this workflow is not primarily caused by these factors. The imprecision of the golden standard of this experiment (the mm paper), which is estimated to have a maximum deviation of 1.0 mm compared to the actual distance, prevents us from drawing further conclusions on the imprecision caused by these sources.

Error caused by the robot and Procrustes algorithm

The two sources of errors which are not a factor in the error test of the stereo camera system, but are factors in the total workflow are the error of the robot and the error of the Procrustes algorithm in finding the underlying transformation $\mathbf{H}_0^c$. The error of the Procrustes algorithm in finding $\mathbf{H}_0^c$ is for a large part dependent on the error of the camera and the robot in determining the tip position of the tool. When the orientation is varied the mean absolute error of the industrial robot is 1.6 mm ($\pm$1.3 SD) which is too large for clinical use. Industrial robots are known to be able to perform motions with a repeatability of up to 1 μm, but to represent their end effector position erroneously in space because of the inaccuracy with which their internal parameters are known. [42, 43] The inaccuracy with which the internal parameters are known causes the robot to represent its end effector position inaccurately in its base frame as the internal parameters such as the length of the robotic links that are used to determine the flange pose with the help of servomotors is not accurately known.

This erroneous representation of the pose of the robotic flange is apparent in the experiment done on this industrial robotic arm. When the joints are altered to reach a variety of different orientations the results are more erroneous 1.6 mm ($\pm$1.3 SD) compared to when the joints are varied minimally when orientation of the tool is kept constant 0.59 mm ($\pm$0.38 SD). When the orientation of the robotic flange is highly varied between measurements the poses of the links are also varied more. And because internal parameters such as the length of the links are inaccurately determined this results in a more erroneous determination of the distance between robotic poses. This inaccuracy of the robotic arm in determining the location of its flange results in a inaccurate and imprecise result while performing the workflow. An inaccurate localization of the robot end effector tip during the registration movements results in a misalignment of F_c to F_0 which in turn leads to inaccurate movements of the robot to target positions on the 3D printed skull. It also results in a imprecision in the measured error as the pose and thus the positional error of the robot is different for every target pose.

6.2 Improving the accuracy in the current setup

6.2.1 Robotic arm

To achieve a more accurate result a robot in which the internal parameters are known with an higher accuracy need to be used. Determining these internal robotic parameters could be achieved by an external calibration procedure. [42, 43] In which the error of the robot could be reduced to a maximum displacement error of less than 0.5 mm and a mean error of 0.208 mm. [42, 43] It could also be achieved by using a robot from which its internal parameters are known beforehand as is done by Ma et al. and the MRSMR robotic system developed by Kong et al. [44, 45] This improvement is likely to have the largest impact on the error of the workflow.

6.2.2 Registration methodology

In the current registration procedure the positions of four reflective spheres on the pointer are used to determine the position of the tip of the pointer in 5 locations. These tip positions are then supplied to the Procrustes algorithm to determine the $\mathbf{H}_0^c$ transformation matrix. In this way 4 measurements are combined to 1 to eventually supply 5 measurements instead of 20 to the Procrustes algorithm. The registration accuracy could be improved by directly supplying the sphere positions determined by the camera to the Procrustes algorithm. In this way imprecisions are less likely to influence the accuracy with which $\mathbf{H}_0^c$ can be found, since measurements are supplied directly to the algorithm without combining measurements beforehand.

6.2.3 Camera setup

In the current setup a stereo camera system with a wide angle lenses is used to get a relatively wide field of view (FOV) at a distance close to the tracking system. For a clinical implementation it would be beneficial if the tracking system is placed at a larger distance from the patient so that the tracking system is not in the way of the surgeons while performing the operation. The surgeons can in this way perform certain procedures and the robot others without having to move the stereo camera setup. The use of lenses with a larger focal length and thus a larger magnification would be suitable for this clinical application since this larger magnification enables the camera setup to be placed further away from the patient. In the current setup a large part of the pixels on the sensors of the cameras is also not used because of the large FOV of the cameras. The pixels that are not used do not contribute to a higher resolution, so narrowing this FOV will result in more pixels on the sensor of each camera being used, and this will thus effectively lead to a higher resolution. Examples of systems that have a smaller FOV but are accurate at a larger distance from the camera due to higher lens magnifications are the 3D tracking systems of Polaris (NDI Ontario, Canada).

For a camera setup that can be applied during an operation a stereo camera system needs to be able to detect the skull during the operation without the presence of reflective markers. Ma et al. applied surface based tracking for movement compensation of a robot by tracking the teeth in the lower jaw to get to know the pose of the mandible using the preoperatively made CT scan. [30] Teeth are exposed ridged extensions of bone which are distinguishable on a CT scan making them a suitable target for surface based tracking. [44] The skull is during an open reconstruction also largely exposed and distinguishable on a CT scan, which opens up the possibility to locate and track this distinguishable shape of the skull. As this 3D structure is known beforehand because of the preoperatively made CT-scan. Whether the tracking of the skull can be done with sufficient accuracy and reliability needs to be investigated. To apply pose tracking, the skull needs to constantly be in the line of sight of both cameras for a reliable tracking. To ensure line of sight the use of more than one stereo camera system is expected to be needed.

6.3 Comparison of workflow with other studies

Registration of the stereo camera system to the robotic system can be achieved by using rigid links from which the transformation for describing one frame with respect to another is known beforehand as done by Ma et al. [44] This is deemed to be less practical for the implementation in craniosynostosis surgery because the entire system would probably need to be repositioned during the surgery with this approach as the entirety of the rigid links with its cameras would be of a hindrance for the surgeons during the operation. This would also entail adjustment of the camera poses during the operation making it less practical for this robotic application. Registration of the stereo camera system to the robotic system can also be achieved by designing a box of reflective fiducial markers, attaching this box to the robot flange and placing this box over the patient as is done in the FDA approved ROSA (Robotized Stereotactic Assistant) (Medtech, Montpellier, France) or by positioning a tool with reflective markers in a variety of poses in the workspace of the robotic system as is done by Kong et al. [45, 46] In the proposed robotic workflow of Kong et al. for a mandible reconstruction it is also required for the robot tip to make contact with titanium screws on a part of the mandibula for patient registration. The workflow of presenting the pose of the tool to the stereo camera system in various orientation was chosen for the robotic implementation of craniosynostosis surgery as this registration step can be performed before the patient is brought in.

Patient registration and tracking can be done with reflective markers attached to the test object or patient as is done by Kong et al. and in the ROSA robotic system or with titanium screws serving as markers for patient registration as is done in the ROBODOC and Caspar surgical systems. [19, 26, 45, 46] Patient registration by means of anatomical landmarks and surface points on the bone is done in the Mazor X surgical system (Medtronic, Dublin, Ireland). [47, 48] Tracking occurs in this surgical system with a combination of fluoroscopic updates and patient tracking by means of reflective markers. [19, 47, 48] In the currect workflow presented in this thesis detection of the 3D printed skull is done using reflective markers. The eventual goal is to replace these reflective markers by a surface based registration and tracking as indicated in section 6.2.3. In the workflow as it is now the localization error can be compared to the error of the ROSA robotic system and the MRSMR robotic system as the way of detecting targets and matching the stereo camera frame to the robotic frame is similar for these 2 systems. The mean error of the ROSA robotic system in placing pedicle screws at the planned position in patients is reported to be 2.05 mm ($\pm$1.2 SD) for the head of the screw, 1.65 mm ($\pm$ 1.11 SD) for the middle of the screw, and 1.57 mm ($\pm$ 1.01 SD) for the tip of the screw. Kong et al. reported a mean placement error of 1.47 mm. [45, 46] The error found in this workflow should be comparable to the error reported in these systems. As explained in section 6.1.2 the larger error found in this workflow is for a large part due to the inaccuracy with which the internal parameters of this robot are known.

6.4 Towards a clinical implementation

6.4.1 Testing movement compensation

An important requirement of performing the operation using a robotic arm is that the robotic arm can compensate for patient movements. This robotic system is set up to allow for the compensation of movements detected by the 3D camera system. For this to be implemented an effective speed and acceleration for the compensation movements by the robot needs to determined. The compensation for patient movements by a robotic arm is applied in the ROSA robotic system, the MSMRN robotic system and by Ma et al. [19, 44–48]

6.4.2 Time and cost effectiveness

As stated in the introduction the surgical operating time is expected to decease with a robotic implementation as the robot can saw the preoperatively determined patterns directly instead of first fitting a guide then drawing the patterns and then sawing while closely following the drawn patterns. It is however to be expected that there is some added preparation time with a robotic approach as the cameras need to be positioned correctly prior to the operation and the robot needs to be integrated within the sterile field of the operation. With the use of a fitting guide these preparation steps are not needed. Surgical operating time is however arguably more valuable than preparation time as a shorter operating time leads to less blood loss and anesthetic usages in this operation. [9] Concerning the cost effectiveness of the robotic implementation it is to be expected that the development and initial purchase costs are considerable higher for a robotic implementation. By eliminating the costs of developing and manufacturing patient specific molds for each operation, and because of the reduction in the costs associated with a reduced operating time of a robotic approach (less anesthetic usages and blood loss) the costs per operation are expected to decrease when a robotic approach is fully implemented within the surgical operation. To make this robotic approach more cost effective than the current approach the robot would however be required to perform a considerable amount of these operations.

6.5 Limitation of experiments

The error of the workflow in reaching the targets on the 3D printed skull is measured by drawing on the surface of this skull. This is an underestimation of the total error in the workflow as the error in the direction perpendicular to the surface of the skull is not taken into account. The error in this direction would however also be less relevant when a force sensor is implemented in the workflow.

The correct tracking of the tip of the pointer on the mm paper from different orientations using the robot and stereo camera system is dependent on the accuracy with which the length of the tool is determined. This length is measured with the before mentioned digital caliper. The measurement of the length of the pointer is not of importance when the tool is brought four times in the same orientation to the mm paper as an inaccurate length determination will not result in any displacements in the direction parallel to the surface while this is the case. The error caused by an inaccurate length determination is expected to be below 0.5 mm. The accuracy with which the length of the pointer is determined only influences the error of the measurements in which the orientation is varied and not the measurements in which the orientation is remained constant to the mm paper. This thus results in an additional overestimation of the error of the experiment in which the orientation is varied with respect to the mm paper which is not present in the measurement in which the orientation is remained constant with respect to the mm paper and is also not present in the error measurement of the entire workflow.

Chapter 7

Conclusion

A robotic workflow for an open cranial vault remodeling for craniosynostosis is developed. Performing a necessary alignment step in a preparation stage and implementing direct communications of the laptop with the stereo camera and robot fits with the requirements of achieving a robotic workflow that is efficient with regards to to the surgical operating time and that has the ability to perform movement compensation. The found mean Euclidean error of 3.9 mm ($\pm$ 0.79 mm SD), 4.0 mm ($\pm$ 1.1 mm SD) and 3.9 ($\pm$ 0.78 mm SD) for three distinct registration trajectories makes the implementation of this workflow in its current form and with the currently used materials not accurate and precise enough for a clinical implementation. The relatively large inaccuracy of the Viper 850 robotic in determining its end effector pose in its base frame is suspected to cause a large part of this error. To increase the accuracy of this workflow it is recommended to replace the used industrial robot with a robot from which its internal parameters are determined with a higher accuracy and to use a stereo camera setup with higher lens magnification and a more narrow FOV so that the tracking system is a better fit for the surgical procedure.

Bibliography

1. Schoenwolf, G. C., Bleyl, S. B., Brauer, P. R. & Francis-West, P. H. *Larsen's human embryology* 4th (Churchill Livingstone, an imprint of Elsevier Inc., 2008).
2. Cornelissen, M. *et al.* Increase of prevalence of craniosynostosis. *Journal of Cranio-Maxillofacial Surgery* **44,** 1273–1279. ISSN: 18784119 (2016).
3. Johnson, D. & Wilkie, A. O. M. Craniosynostosis. *European Journal of Human Genetics* **19,** 369–376. ISSN: 10184813 (2011).
4. Buchanan, E. P., Xue, Y., Xue, A. S., Olshinka, A. & Lam, S. *Multidisciplinary care of craniosynostosis* 2017.
5. Honeycutt, J. H. Endoscopic-assisted craniosynostosis surgery. *Seminars in Plastic Surgery* **28,** 144–149. ISSN: 15360067 (2014).
6. Chim, H., Wetjen, N. & Mardini, S. Virtual surgical planning in craniofacial surgery. *Seminars in Plastic Surgery* **28,** 150–157. ISSN: 15360067 (2014).
7. Andrew, T. W. *et al.* Virtual surgical planning decreases operative time for isolated single suture and multi-suture craniosynostosis repair. *Plastic and Reconstructive Surgery - Global Open* **6.** ISSN: 21697574. `/pmc/articles/PMC6326593/%20/pmc/articles/PMC6326593/?report=abstract%20https://www.ncbi.nlm.nih.gov/pmc/articles/PMC6326593/` (2018).
8. Ali, A. *et al.* Factors influencing blood loss and postoperative morbidity in children undergoing craniosynostosis surgery: A retrospective study. *Pediatric Neurosurgery* **49,** 339–346. ISSN: 14230305. `https://pubmed.ncbi.nlm.nih.gov/25472759/` (Feb. 2013).
9. Seruya, M. *et al.* Factors related to blood loss during fronto-orbital advancement. *Journal of Craniofacial Surgery* **23,** 358–362. ISSN: 10492275. `https://pubmed.ncbi.nlm.nih.gov/22421855/` (Mar. 2012).
10. Faberowski, L. W., Black, S. & Mickle, J. P. Blood loss and transfusion practice in the perioperative management of craniosynostosis repair. *Journal of Neurosurgical Anesthesiology* **11,** 167–172. ISSN: 08984921. `https://pubmed.ncbi.nlm.nih.gov/10414670/` (1999).
11. Bussink, T. *Augmented reality in cranio-maxillofacial surgery* PhD thesis (Twente University, 2020), 60.
12. Seruya, M. *et al. Computer-aided design and manufacturing in craniosynostosis surgery* in *Journal of Craniofacial Surgery* **24** (2013), 1100–1105.
13. Soleman, J., Thieringer, F., Beinemann, J., Kunz, C. & Guzman, R. Computer-assisted virtual planning and surgical template fabrication for frontoorbital advancement. *Neurosurgical Focus* **38.** ISSN: 10920684 (2015).
14. Kobets, A. J. *et al.* Virtual modeling, stereolithography, and intraoperative CT guidance for the optimization of sagittal synostosis reconstruction: a technical note. *Child's Nervous System* **34,** 965–970. ISSN: 14330350 (2018).

15. Meulstee, J. W. *EVALUATION OF THE CRANIAL VAULT IN NEWBORNS* PhD thesis (Twente University, 2013).

16. Siepel, F. J. *et al.* Needle and Biopsy Robots: a Review. *Current Robotics Reports,* 1–12. `https://doi.org/10.1007/s43154-020-00042-1` (2021).

17. Klein, M. I. *et al.* Mental stress experienced by first-year residents and expert surgeons with robotic and laparoscopic surgery interfaces. *Journal of Robotic Surgery* **8,** 149–155. ISSN: 18632483. `https://link.springer.com/article/10.1007/s11701-013-0446-8` (2014).

18. Moustris, G. P., Hiridis, S. C., Deliparaschos, K. M. & Konstantinidis, K. M. Evolution of autonomous and semi-autonomous robotic surgical systems: A review of the literature. *International Journal of Medical Robotics and Computer Assisted Surgery* **7,** 375–392. ISSN: 14785951 (2011).

19. Hill, D., Williamson, T., Lai, C. Y., Leary, M. & Brandt, M. Robots and tools for remodeling bone. *IEEE Reviews in Biomedical Engineering* **13,** 184–198. ISSN: 19411189 (2020).

20. Yang, G.-Z. *et al.* Medical robotics-Regulatory, ethical, and legal considerations for increasing levels of autonomy. `http://robotics.sciencemag.org/`.

21. Ficuciello, F., Tamburrini, G., Arezzo, A., Villani, L. & Siciliano, B. Autonomy in surgical robots and its meaningful human control. *Paladyn* **10,** 30–43. ISSN: 20814836 (2019).

22. Yip, M. & Das, N. *Robot autonomy for surgery* 2017.

23. Van Der Schatte Olivier, R. H., Van't Hullenaar, C. D. P., Ruurda, J. P. & Broeders, I. A. M. J. Ergonomics, user comfort, and performance in standard and robot-assisted laparoscopic surgery. *Surgical Endoscopy* **23,** 1365–1371. ISSN: 14322218. `https://link.springer.com/article/10.1007/s00464-008-0184-6` (2009).

24. Vo, C. D. *et al.* Robotic Spine Surgery: Current State in Minimally Invasive Surgery. *Global Spine Journal* **10,** 34S–40S. ISSN: 21925690. `https://us.sagepub.com/en-us/nam/open-access-at-sage` (2020).

25. Kayani, B., Konan, S., Tahmassebi, J., Pietrzak, J. R. T. & Haddad, F. S. Robotic-arm assisted total knee arthroplasty is associated with improved early functional recovery and reduced time to hospital discharge compared with conventional jig-based total knee arthroplasty. *The Bone & Joint Journal* **100-B,** 930–937. ISSN: 2049-4394. `https://online.boneandjoint.org.uk/doi/10.1302/0301-620X.100B7.BJJ-2017-1449.R1` (2018).

26. Pransky, J. ROBODOC - surgical robot success story. *Industrial Robot* **24,** 231–233. ISSN: 0143991X (1997).

27. Liow, M. H. L. *et al.* Early experiences with robot-assisted total knee arthroplasty using the digiMatch^{TM} ROBODOC®surgical system. *Singapore Medical Journal* **55,** 529–534. ISSN: 00375675. `/pmc/articles/PMC4293963/%20/pmc/articles/PMC4293963/?report=abstract%20https://www.ncbi.nlm.nih.gov/pmc/articles/PMC4293963/` (2014).

28. Siebert, W., Mai, S., Kober, R. & Heeckt, P. F. Technique and first clinical results of robot-assisted total knee replacement. *Knee* **9,** 173–180. ISSN: 09680160 (2002).

29. Shademan, A. *et al.* Supervised autonomous robotic soft tissue surgery. *Science Translational Medicine* **8,** 64–337. ISSN: 19466242. `www.iso.org` (2016).

30. Ma, Q. *et al.* Development and preliminary evaluation of an autonomous surgical system for oral and maxillofacial surgery. https://doi.org/10.1002/rcs.1997 (2019).

31. Varma, T. R. K. & Eldridge, P. *Use of the NeuroMate stereotactic robot in a frameless mode for functional neurosurgery* 2006. https://pubmed.ncbi.nlm.nih.gov/17520621/.

32. Groenhuis, V., Veltman, J., Siepel, F. J. & Stramigioli, S. Stormram 3: A magnetic resonance imaging-compatible robotic system for breast biopsy. *IEEE Robotics and Automation Magazine* **24,** 34–41. ISSN: 10709932 (2017).

33. Salvi, J., Armangué, X. & Batlle, J. A comparative review of camera calibrating methods with accuracy evaluation. *Pattern Recognition* **35,** 1617–1635. ISSN: 00313203 (July 2002).

34. Ramírez-Hernández, L. R. *et al.* Improve three-dimensional point localization accuracy in stereo vision systems using a novel camera calibration method. *International Journal of Advanced Robotic Systems* **17,** 172988141989671. ISSN: 1729-8814. http://journals.sagepub.com/doi/10.1177/1729881419896717 (Jan. 2020).

35. PS-tech. *Optical Tracking Explained* 2021. https://www.ps-tech.com/optical-tracking-explained/.

36. Van Wyk, K. & Marvel, J. A. Strategies for Improving and Evaluating Robot Registration Performance. *IEEE Transactions on Automation Science and Engineering* **15,** 320–328. ISSN: 15455955 (2018).

37. Pilon, A. J. M. *et al. Robot-guided translation of a preoperative 3D planning during open-vault reconstruction of craniosynostosis* tech. rep. (RadboudUMC, Twente University, 2019).

38. Gower, J. C. A General Coefficient of Similarity and Some of Its Properties. *Biometrics* **27,** 857. ISSN: 0006341X (Dec. 1971).

39. Zhou, Z. *et al.* Optical surgical instrument tracking system based on the principle of stereo vision. *Journal of Biomedical Optics* **22,** 65005. ISSN: 1083-3668. http://biomedicaloptics.spiedigitallibrary.org/article.aspx?doi=10.1117/1.JBO.22.6.065005 (2017).

40. Haidegger, T., Benyö, B., Kovács, L. & Benyö, Z. *Force sensing and force control for surgical robots* in *IFAC Proceedings Volumes (IFAC-PapersOnline)* **7** (Elsevier, 2009), 401–406. ISBN: 9783902661494.

41. Kim, U., Lee, D. H., Kim, Y. B., Seok, D. Y. & Choi, H. R. A novel six-axis force/torque sensor for robotic applications. *IEEE/ASME Transactions on Mechatronics* **22,** 1381–1391. ISSN: 10834435 (2017).

42. Gaudreault, M., Joubair, A. & Bonev, I. Self-Calibration of an Industrial Robot Using a Novel Affordable 3D Measuring Device. *Sensors* **18,** 3380. ISSN: 1424-8220. http://www.mdpi.com/1424-8220/18/10/3380 (Oct. 2018).

43. Švaco, M., Šekoranja, B., Šuligoj, F. & Jerbić, B. *Calibration of an industrial robot using a stereo vision system* in *Procedia Engineering* **69** (Elsevier Ltd, 2014), 459–463.

44. Ma, Q. *et al.* Autonomous Surgical Robot with Camera-Based Markerless Navigation for Oral and Maxillofacial Surgery. *IEEE/ASME Transactions on Mechatronics* **25,** 1084–1094. ISSN: 1941014X (2020).

45. Kong, X. Z., Duan, X. G. & Wang, Y. G. An integrated system for planning, navigation and robotic assistance for mandible reconstruction surgery. *Intelligent Service Robotics* **9,** 113–121. ISSN: 18612784 (2016).

46. Lefranc, M. & Peltier, J. Evaluation of the ROSA^{TM} Spine robot for minimally invasive surgical procedures. *Expert Review of Medical Devices* **13,** 899–906. ISSN: 17452422. `https://www.tandfonline.com/doi/full/10.1080/17434440.2016.1236680` (Oct. 2016).

47. D'Souza, M. *et al.* Robotic-Assisted Spine Surgery: History, Efficacy, Cost, And Future Trends. *Robotic Surgery: Research and Reviews* **Volume 6,** 9–23. ISSN: 2324-5344. `/pmc/articles/PMC6844237/%20/pmc/articles/PMC6844237/?report=abstract%20https://www-ncbi-nlm-nih-gov.ezproxy2.utwente.nl/pmc/articles/PMC6844237/` (Nov. 2019).

48. Vadalà, G. *et al. Robotic spine surgery and augmented reality systems: A state of the art* Mar. 2020. `/pmc/articles/PMC7136092/%20/pmc/articles/PMC7136092/?report=abstract%20https://www.ncbi.nlm.nih.gov/pmc/articles/PMC7136092/`.